

# Development of DDES and IDDES Formulations for the $k$ - $\omega$ Shear Stress Transport Model

Mikhail S. Gritskevich · Andrey V. Garbaruk ·  
Jochen Schütze · Florian R. Menter

Received: 18 April 2011 / Accepted: 24 October 2011  
© Springer Science+Business Media B.V. 2011

**Abstract** Modifications are proposed of two recently developed hybrid CFD strategies, Delayed Detached Eddy Simulation (DDES) and DDES with Improved wall-modeling capability (IDDES). The modifications are aimed at fine-tuning of these approaches to the  $k$ - $\omega$  SST background RANS model. The first one includes recalibrated empirical constants in the shielding function of the SA-based DDES model which are shown to be suboptimal (not providing the needed level of elimination of the Model Stress Depletion (MSD)) for the SST-based DDES model. For the SST-IDDES variant, in addition to that, a simplification of the original SA-based formulation is proposed, which does not cause any visible degradation of the model performance. Both modifications are extensively tested on a range of attached and separated flows (developed channel, backward-facing step, periodic hills, wall-mounted hump, and hydrofoil with trailing edge separation).

**Keywords** LES · Delayed detached eddy simulation · DDES · Improved delayed detached eddy simulation · IDDES · Wall modeling in LES · WMLES

## 1 Introduction

Industrial CFD simulations increasingly rely on Scale-Resolving Simulation (SRS) models, which resolve at least a part of the turbulence spectrum in at least a part of the flow domain. Due to the excessive costs of classical Large Eddy Simulation (LES) for high-Reynolds number industrial simulations, hybrid and/or zonal RANS-LES models are quickly becoming the models of choice for such applications.

---

M. S. Gritskevich (✉) · A. V. Garbaruk  
St. Petersburg State Polytechnical University, 195251, St. Petersburg, Russia  
e-mail: gritskevich@yandex.ru

J. Schütze · F. R. Menter  
Software Development Department, ANSYS, 83714, Otterfing, Germany

A result of the intensive research in this area, a significant number of models have been proposed in recent years [1] making a comparison and selection of the most appropriate model a daunting task. However, only a small number of model formulations are used in today's industrial CFD codes and can roughly be categorized in the following way:

- Improved Unsteady RANS (URANS) models which allow the formation of resolved turbulent structures in unstable flows without an explicit impact of the grid spacing on the RANS model formulation. The most widely used model of this type is the Scale-Adaptive Simulation (SAS) variant. These models are relatively safe to use, as they provide a RANS/URANS fallback position for under-resolved grids and/or time steps. On the downside, such models require relatively strong flow instabilities in order to switch to SRS mode.
- Detached Eddy Simulation (DES) models, which switch explicitly between RANS and LES model formulations based on the local grid spacing and turbulent length scale. The original intent of DES was to be run in RANS mode for attached boundary layers and to switch to LES mode in large separated (detached) flow regions. The explicit switch to the LES model is however not accompanied by a corresponding transfer of modeled (RANS) turbulence to resolved (LES) turbulence. As with SAS, DES relies on inherent flow instability for a quick generation of such resolved content. Due to the direct impact of the grid spacing on the RANS model, DES models require more carefully crafted grids to avoid inappropriate behavior. On the other hand, DES models allow a local reduction in eddy-viscosity by grid refinement in the 'transition' region between RANS and LES, which in turn can help in the formation of unsteady content, for flows where models like SAS would remain in RANS/URANS mode.
- Wall Modeled LES (WMLES) models, which aim at reducing the strong Reynolds number dependency of classical LES for wall-bounded flows. This is typically achieved by covering only the inner-most part of the boundary layer in RANS mode and resolving most of the turbulence inside the boundary layer by LES techniques. This avoids the need of resolving the smallest and most Reynolds number dependent turbulent eddies above the viscous sublayer. As the turbulent eddies inside the attached boundary layer are typically still much smaller than 'detached' eddies, WMLES requires a substantially higher computational effort than classical DES.
- Zonal (or embedded) LES models, where the user divides the domain into separate regions where RANS and LES models are applied respectively. At the Interface between an upstream RANS and a downstream LES region, synthetic turbulence is typically inserted into the simulation, providing a clear transfer of turbulence energy from modeled to resolved content. Obviously, zonal formulations can be combined with the use of a WMLES formulation in the 'LES' zone.

The current article will focus on different aspects and variants of the DES model formulation. While the original DES model is straightforward and simple, DES is nevertheless one of the more difficult models to use in complex applications. The user requires not only a basic understanding of the model behavior, but also has to follow relatively intricate grid generation guidelines to avoid undefined simulation behavior somewhere between RANS and LES. In addition, several variants of the DES model,

like Delayed DES (DDES) and Improved DDES (IDDES) have been proposed with rather different characteristics, making model selection and interpretation of results challenging.

Problematic behavior of standard DES has been reported by Menter and Kuntz [2] who demonstrated that an artificial separation could be produced for an airfoil simulation when refining the max cell edge length ( $h_{\max}$ ) inside the wall boundary layer below a critical value of  $h_{\max}/\delta < 0.5\sim 1$ , where  $\delta$  is the local boundary layer thickness. This effect was termed Grid Induced Separation (GIS) as the separation depends on the grid spacing and not the flow physics. GIS is obviously produced by the effect of a sudden grid refinement which changes the DES model from RANS to LES, without balancing the reduction in eddy-viscosity by resolved turbulence content. Spalart [3] coined the term Modeled Stress Depletion (MSD) which refers generally to the effect of reduction of eddy-viscosity from RANS to LES without a corresponding balance by resolved turbulent content. In other words, GIS is a result of MSD. MSD is essentially a result of insufficient flow instabilities downstream of the switch from the RANS to the LES model formulation. Especially for wall bounded flows, the flow instability is too weak and it would require many boundary layer thicknesses to allow the formation of a sufficiently developed turbulent LES content to balance the reduction of the RANS model. For that reason, the switch from the RANS to the LES model inside wall boundary layers is not desirable. GIS can in principle be avoided by shielding the RANS model from the DES formulation for wall boundary layers. This was proposed by Menter and Kuntz, who used the blending functions of the SST model [2] for that purpose. Later, Spalart et al. [3] proposed a more generic formulation of the shielding function, which depends only on the eddy-viscosity and the wall distance. It can therefore, in principle, be applied to any eddy-viscosity based DES model. The resulting formulation was termed Delayed Detached Eddy Simulation (DDES) [3]. While the shielding function developed in [3] was considered generic, it was essentially calibrated for the Spalart-Allmaras (SA) one-equation RANS model.

It will be shown that a recalibration is required if the same function is to be applied to other models like the SST two-equation model used in the current work. It is important to emphasize that the development and/or calibration of DDES shielding functions requires a delicate balance between the need of shielding the boundary layer and the desire of not inhibiting the formation of turbulent structures in the ‘transition’ zone between attached (RANS) and detached (LES) flow. Overly conservative shielding would allow a high degree of mesh refinement inside the boundary layer without any impact on the RANS model, but would suppress the formation of resolved turbulence in detached flow regions not sufficiently removed from walls (e.g. backward facing step flows, tip gap flows in axial turbines, etc.). Due to the limited shielding provided by the original DDES function for the SST model, the current implementation in the ANSYS CFD solvers offers a choice of the F1 and F2 blending functions of the SST model and the original DDES shielding function of Spalart [3]. The default is the relatively conservative F2 function (actually 1-F2 in current notation). It is one of the goals of this article to avoid the ambiguity of numerous shielding functions and to consolidate the SST-DDES approach.

Another interesting aspect spurring many discussions and model enhancements resulted from the application of the original DES model as a WMLES formulation.

Obviously this was not the original intent of the model, and it resulted in a relatively strong Logarithmic Layer Mismatch (LLM) between the inner RANS and the outer LES regions. Nevertheless, these tests indicated that DES could be developed into a suitable WMLES formulation, resulting in the formulation of the IDDES model, Shur et al. [4]. The IDDES model features several rather intricate blending and shielding functions, which allow using this model both in DDES and WMLES mode. These functions will be revisited, again in combination with the SST model, and some recalibration and simplifications will be proposed, in an attempt of making the model both simpler and more reliable.

## 2 Brief Description of the Numerics

All the simulations in the present study have been carried out with the use of the ANSYS-Fluent 13 CFD code [5]. For all the considered flows, the incompressible fluid assumption was selected. A finite volume method on unstructured grids with a cell-centered data arrangement was adopted.

The equations are solved with the use of the implicit point Gauss-Seidel method with a Rhie-Chow flux correction [6] which is aimed at suppressing unphysical pressure oscillations. An algebraic multigrid approach is applied for convergence acceleration by computing corrections on a series of grids. For the RANS computations, the coupled steady state solver [5] is employed, whereas for DDES and IDDES, a non-iterative time advancement procedure [7, 9, 10] is used which allows integrating the governing equations in time without inner iterations on each time step.

The inviscid fluxes are approximated with the use of the second order upwind scheme [5] for RANS and with the second order centered scheme [5] for DDES and IDDES. The time derivatives in the latter simulations are approximated with the use of the three-layer second order backward Euler scheme.

## 3 Recalibration of the Original DDES Constants to the $k$ - $\omega$ SST Model

The original SST-DDES formulation combines the SST-DES formulation of Strelets [11] with the DDES shielding functions of Spalart et al. [3]. The original SST-DES model starts to decrease the eddy viscosity for  $h_{\max}/\delta < 0.8$  and the purpose of the empirical shielding function is to preserve the eddy viscosity from degradation up to  $h_{\max}/\delta = 0.1$  (in fact even less). The empirical delay function  $f_d$  involved in the DDES approach reads as follows [3]:

$$f_d = 1 - \tanh \left[ \frac{(C_{d1} r_d)^{C_{d2}}}{v_t + \nu} \right]$$

$$r_d = \frac{\nu_t + \nu}{\kappa^2 d_w^2 \sqrt{0.5 \cdot (S^2 + \Omega^2)}}$$

Here  $\nu_t$  and  $\nu$  are the eddy and molecular viscosities respectively,  $S$  and  $\Omega$  are strain rate and vorticity tensor invariants,  $\kappa = 0.41$  is the von Karman constant, and  $d_w$  is the distance to the wall. The DES limiter is deactivated if the function  $f_d = 0$ . For a full description of the DDES model see Appendix 1.

Based on the computations of a zero-pressure-gradient boundary layer with the use of the SA RANS model and SA-based DDES carried out in Spalart et al. [3] on a fairly ambiguous grid (with a target value of the grid-spacing equal to one tenth of the boundary layer thickness) the values of the constants  $C_{d1}$  and  $C_{d2}$  involved in the quantity  $r_d$  have been set equal to 8 and 3 respectively. However, as shown in Fig. 1a, profiles of  $r_d$  are different for the SA-DDES and SST-DDES models when using the same shielding function. Thus, with these values of the constants, the SST-DDES delay function turns out to be equal to 1 in a significantly narrower domain than the SA-DDES function, which results in a less-reliable shielding of the boundary layer for SST-based DDES compared to SA-based DDES (see Fig. 1b).

A series of SST-based DDES computations with different values of the constants has shown that, in order to ensure nearly the same protection of the SST-based DDES model from a premature switching to LES mode as for the SA-based DDES model, the value of  $C_{d1}$  should be set to 20, whereas the constant  $C_{d2}$  should be kept the same as in the SA-based DDES (see Fig. 1b). A significant decrease of the  $f_d$  function is explained by low values of strain rate magnitude (is used in denominator of the  $r_d$  criterion) near  $y/\delta \approx 1.2$ . Note that this will not affect the BL as it happens outside the BL, thus the decrease should not cause any problems.

A significant improvement of the SST-based DDES performance on ambiguous grids ensured by the use of the new set of the constants is illustrated by Fig. 2a, b. The figures present results of the SST-DDES model for the flat plate boundary layer computed in RANS mode with the DDES option activated. In this simulation the maximum grid-spacing  $h_{max}$ , involved in the DDES formulation was abruptly changed from  $\delta$  (boundary layer thickness at  $Re_x = 10^7$ ) to  $0.1 \cdot \delta$  at  $Re_x = 5 \cdot 10^6$ . This situation may well be the case in complex flows, e.g. in the vicinity of geometry singularity. As seen in Fig. 2a for the SST-based DDES model with the “standard” (recommended for the SA-based DDES) value of the  $C_{d1} = 8$ , the shielding of the

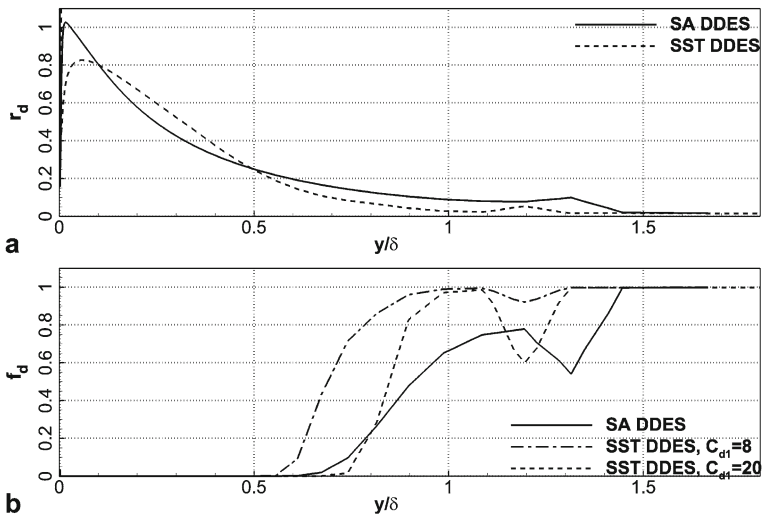


**Fig. 1** Comparison between SA- and SST-based DDES for flat plate boundary layer: **a**— $r_d$  quantity, **b**— $f_d$  shielding function

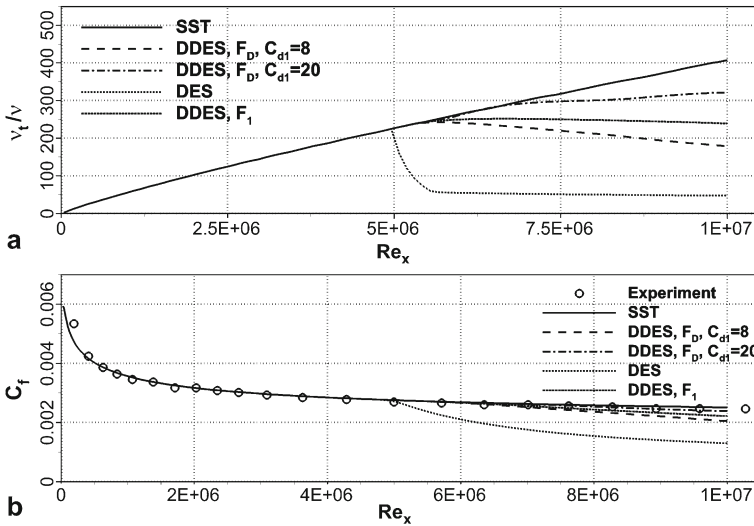


**Fig. 2** Effect of  $C_{d1}$  constant on the flat plate flow predicted by SST-based DDES: **a**—distribution of eddy viscosity maximum value in each profile over the plate, **b**—distribution of skin friction coefficient over the plate

model from the premature switching inside the boundary layer to the LES mode typical for the original DES is not completely eliminated. A significant drop of the maximum eddy viscosity per profile compared to the SST RANS eddy viscosity is observed (see Fig. 2a). This naturally leads to a tangible deviation of the friction coefficient from the SST RANS curve (Fig. 2b) and more importantly could result in GIS under adverse pressure gradient conditions. In contrast to this, with  $C_{d1} = 20$ , both eddy viscosity and skin friction predicted by the SST DDES are virtually the same as those computed with the SST RANS model for a longer running length of the boundary layer. Even with the new limiter, the RANS mode for boundary layer computations will be affected once  $h_{max}/\delta < 0.1$ . This can be seen to happen for the current grid at  $Re_x \sim 7 \cdot 10^6$  (see Fig. 2a). This is a general property of all DDES models and is a consequence of the balance between the desire to provide as much shielding as possible and not to inhibit the scale-resolving capability of the DES approach.

Overly conservative shielding of the DES model can, in principle, result in impairing the turbulence resolving capability of the DDES model in separated flow regions. In order to make sure that this does not occur with  $C_{d1} = 20$ , the backward-facing step flow of Vogel and Eaton [10] has been computed. In this flow, the Reynolds number based on the bulk velocity and on the step height  $H$  is equal to 28000, and the height of the channel upstream of the step is equal to  $4H$ .

Following previous simulations of this flow using the SA-based DES and DDES [3, 6, 12] models, the computational domain (see Fig. 3a) in the present study extended from  $-3.8H$  to  $20H$  in streamwise direction ( $x = 0$  corresponds to the step location). In the spanwise direction, the size of the domain was  $4H$ .

At the inlet distributions of velocity and turbulence quantities were specified, which were obtained from a precursor calculation conducted in the channel flow and corresponds to experimental value of the boundary layer thickness at that location.

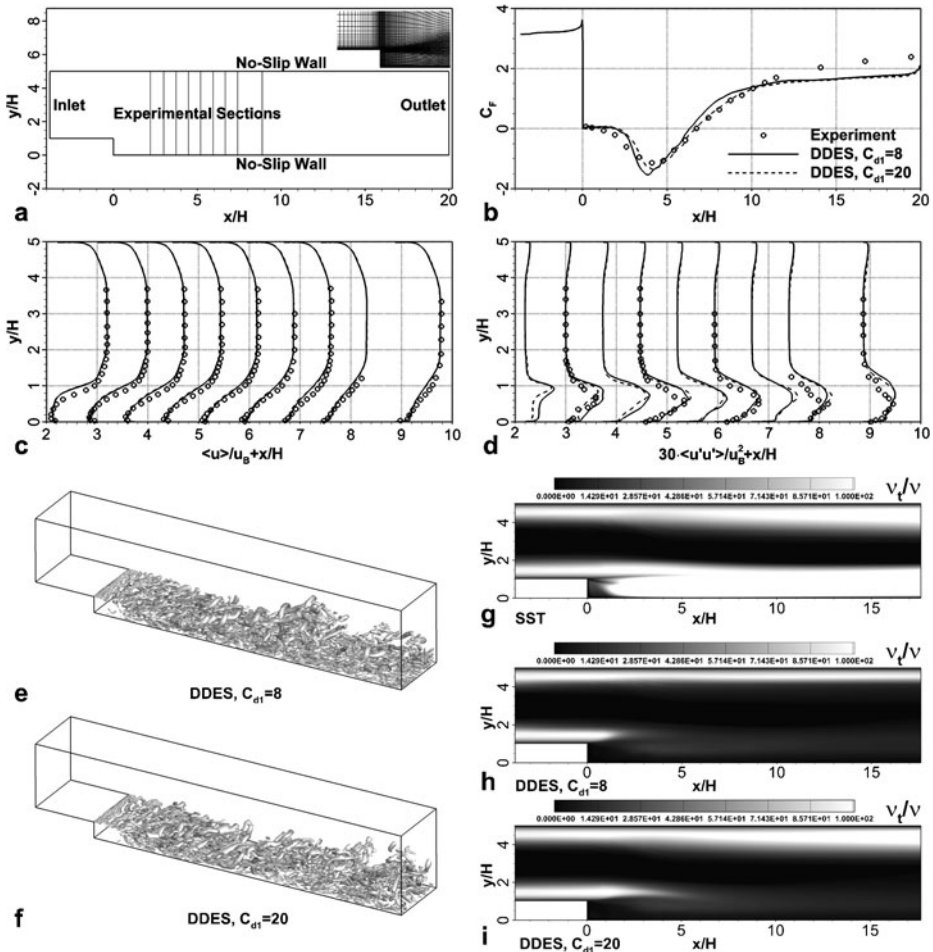


**Fig. 3** A sketch of the flow and a fragment of the computational grid near the separation zone **a** and the effect of the  $C_{d1}$  constant on the BFS mean flow predicted by SST-based DDES: **b**—skin friction coefficient distribution over the step-wall, **c** and **d**—profiles of streamwise velocity  $\langle u \rangle$  and  $\langle u'u' \rangle$  stress, **e** and **f**—iso-surfaces of  $Q$ -criterion equal to  $1 [s^{-2}]$ , **g**, **h**, **i**—contour of eddy viscosity for SST model, DDES with  $C_{d1} = 8$  and DDES with  $C_{d1} = 20$  respectively. Profiles are plotted at  $x/H = 2.2, 3.0, 3.7, 4.5, 5.2, 5.9, 6.7, 7.4, 8.7$

On the outlet boundary a constant pressure was specified. In spanwise direction a periodic conditions were applied.

The computational grid used in the simulation had 2.25 million hexahedral cells (2.3 million nodes) providing a near-wall resolution in wall units to be less than one. A non-dimensional time step of  $\Delta t = 0.02$  was used, ensuring a CFL number of less than one in the entire domain. The number of cells in the spanwise direction was 80. At the inlet, steady state RANS profiles were imposed and unsteadiness results from the inherent flow instability past the step.

Figure 3e, f shows turbulent structures visualized by an iso-surface of the  $Q$ -criterion. It can be seen that these structures develop quickly downstream of the step

in agreement with the expectations for the DDES model approach. Visualizations of turbulent structures of the SST-based DDES solutions obtained with  $C_{d1}$  equal to 8 and 20 have not revealed any visible difference, but a value of  $C_{d1}$  equal to 25 suppressed the resolved turbulence. Such a high value would therefore be overly conservative and inhibit the main DES functionality.

To check the protection of the boundary layer in case of pressure gradients, a comparison of eddy viscosity contours for both  $C_{d1}$  values was performed with the RANS-SST model (see Fig. 3g, h, i). As can be seen, the eddy viscosity on the upper straight wall is significantly decreased in case of DDES with  $C_{d1} = 8$ , while for  $C_{d1} = 20$ , the eddy viscosity is very close to the RANS-SST model.

A comparison of the mean flow characteristics predicted by the two simulations with each other and with the experimental data [10], is presented in Fig. 3b, c, d (experimental sections are presented in Fig. 3a). As seen in the figure, the difference between the friction distributions over the step-wall and velocity fields computed with the different values of the constant is marginal, and both solutions agree well with the data. Thus, the increase of the  $C_{d1}$  constant from 8 to 20 does not cause any noticeable degradation of the SST-based DDES model in LES mode and can be considered as both robust (ensuring a sufficient shielding of SST-DDES from MSD in the attached flow regions) and safe (not leading to a degradation of turbulence resolving capabilities of the model) in the separation regions.

#### 4 Optimization of the IDDES Model Formulation for the SST Model

The IDDES approach [4] presents a combination of DDES with another hybrid model aimed at Wall-Modeled LES (WMLES). In this combined approach, the empiric function providing shielding of the DDES branch of the model from MSD is similar to the function  $f_d$  in DDES and reads as follows [4]:

$$f_{dt} = 1.0 - \tanh \left[ (C_{dt1} \cdot r_{dt})^{C_{dt2}} \right]$$

Here the values of the constants  $C_{dt1}$  and  $C_{dt2}$  are the same as those in the SA-DDES, i.e. 8 and 3 respectively [4]. Thus, taking into account the results presented in Section 3, for the SST-based IDDES, the value of  $C_{dt1}$  constant should also be set to 20. In order to ensure that this does not damage the wall-modeling capability of the IDDES branch, simulations have been carried out for the developed flow in a plane channel, where the wall-modeling capability is essential for computing flows at high Reynolds numbers. In order to also test the model in a flow where both of its branches (DDES and WMLES) are active, the simulation of the BFS presented in the previous section was repeated with the use of the SST-based IDDES.

##### 4.1 Developed channel flow

Simulations of this flow were carried out at the same Reynolds numbers based on friction velocity  $u_\tau$  and channel height  $H$  as those in the SA-IDDES in [4], namely, 395, 2400 and 18000. The flow was driven with a constant pressure gradient  $dp/dx = -2 \cdot \rho \cdot u_\tau^2 / H$ , where  $p$  is the pressure and  $\rho$  is the density. This pressure gradient was taken into account in the governing equation via a source term in the momentum equations and periodic boundary conditions were imposed not only in the spanwise

direction  $z$ , but also in the streamwise direction  $x$ . Note that within such an approach, the bulk velocity of the flow is not specified and should be obtained as a part of the solution, which means that it could be different with different turbulence models. The computational domain used in the present study was also the same as that used in [4], namely, its size was equal to  $4H$  in the streamwise direction and  $1.5H$  in the spanwise direction. For all the considered Reynolds numbers, the computational grid was the same in streamwise and spanwise directions with the grid-spacing of  $0.05H$  and  $0.025H$  respectively which corresponds to  $(\Delta x/\delta, \Delta z/\delta) = (0.1, 0.05)$ . In wall units the grid parameters for different Reynolds numbers are  $(\Delta x^+, \Delta y^+) = (40, 20)$  for  $Re_\tau = 395$ ,  $(\Delta x^+, \Delta y^+) = (240, 120)$  for  $Re_\tau = 2400$ , and  $(\Delta x^+, \Delta y^+) = (1800, 900)$  for  $Re_\tau = 18000$ . For the lowest Reynolds number the grid corresponds to well-resolved LES, while for higher Reynolds numbers the grid requires WMLES. In the wall normal direction, different grids were used providing a sufficient resolution ( $\Delta y_w^+ < 1$  near the wall) at different Reynolds numbers. The non-dimensional time

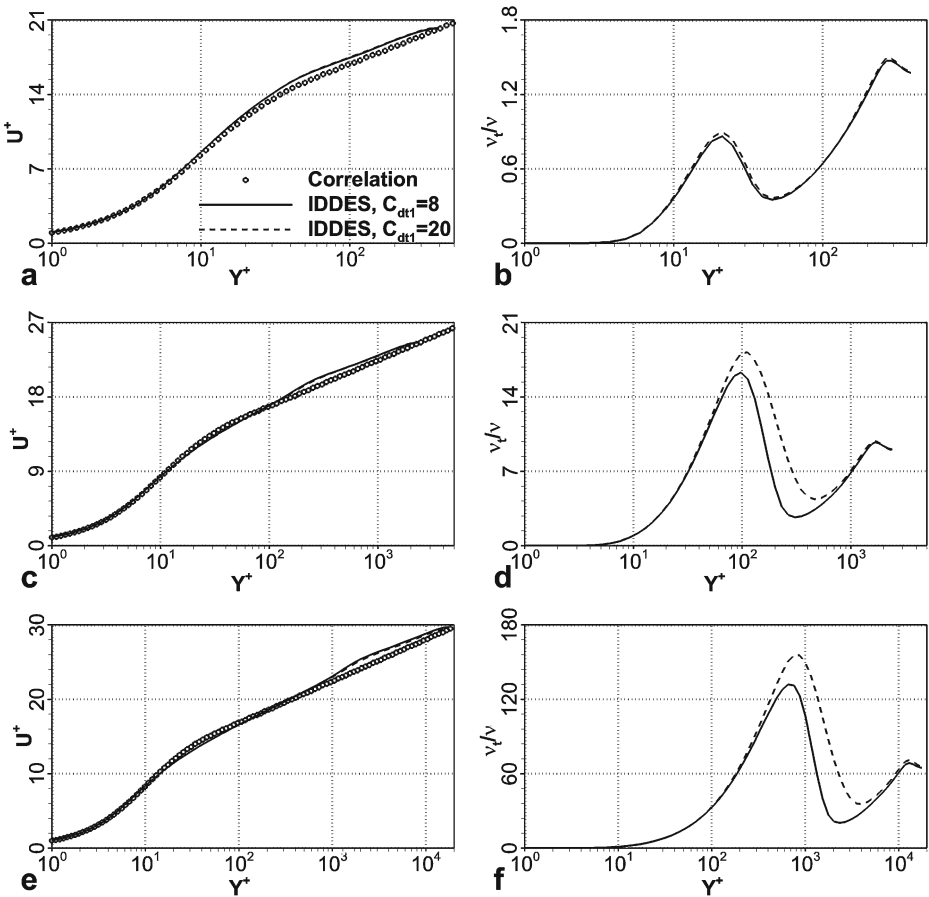


**Fig. 4** Effect of  $C_{drl}$  constant on the SST IDDES simulation of developed channel flow: velocity and eddy viscosity profiles at different Reynolds number: **a, b**— $Re_\tau = 395$ , **c, d**— $Re_\tau = 2400$ , **e, f**— $Re_\tau = 18000$

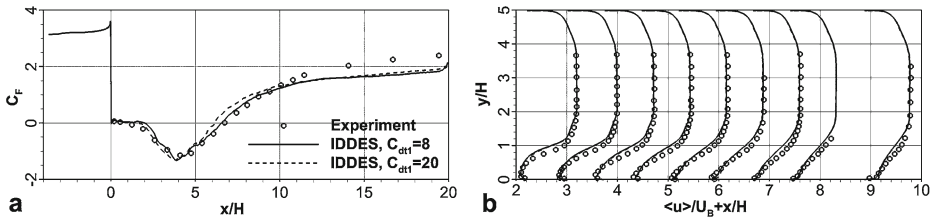


**Fig. 5** An effect of  $C_{dt1}$  constant on the SST IDDES of the BFS flow: **a**—skin friction coefficient distribution, **b**—profiles of streamwise velocity  $\langle u \rangle$ . Profiles are plotted at  $x/H = 2.2, 3.0, 3.7, 4.5, 5.2, 5.9, 6.7, 7.4, 8.7$

step was  $\Delta t = 0.02$  which ensured the CFL number to be less than one in the entire domain.

Results of the simulations obtained with the use of the SST-IDDES model with two values of the constant  $C_{dt1}$  and their comparison with the empirical correlation of Reichart [12] are presented in Fig. 4, where the mean velocity and eddy viscosity profiles for different Reynolds numbers are depicted. It can be seen that the effect of changing  $C_{dt1}$  on these profiles is negligible which suggests that the new value of the constant does not cause any damage to the wall-modeling capability of the SST-based IDDES formulation.

For this case, the grid influence was investigated. For that purpose a grid refined in every spatial direction with a factor of 1.5 was considered. It was shown that both models yield virtually identical results on each grids (the results are not shown here), and thus providing an indication of grid robustness of the solution.

#### 4.2 Backward-facing step flow

As mentioned above, in this flow both branches of IDDES, RANS and WMLES, were active: the model effectively performs in RANS mode in the attached flow region upstream of the step and in the attached boundary layer on the upper straight wall of the channel and as WMLES in the recirculation zone and downstream of the reattachment on the step-wall. The RANS mode was achieved by the shielding function  $f_d$ . The WMLES unsteady content was triggered by the flow instability of the separating shear layer past the step (see also Fig. 3). Results of the SST-IDDES model with  $C_{dt1} = 8$  and  $C_{dt1} = 20$  are depicted in Fig. 5. The figure suggests that the variation of the constant does not affect the performance of the model and yields virtually identical results for all considered quantities. The only visible difference is seen in the skin friction coefficient, but it is also marginal. Other than that, the version of SST-IDDES with the new value of the  $C_{dt1} = 20$  provides very good agreement with the experiment thus supporting the credibility of the proposed modification of the model.

### 5 Simplification of SST-based IDDES

In addition to the delay function discussed above, the IDDES approach involves an elevating-function  $f_e$ , aimed at preventing an excessive reduction of the RANS

Reynolds stresses typically observed in the vicinity of the RANS and LES interface and causing the so-called Log-layer Mismatch (LLM) [4] in both DES and DDES when the models are applied to attached flows. As shown in [4], within the SA-IDDES model this function is more “aggressive” than within the SST-IDDES model, meaning it elevates the RANS model eddy-viscosity more strongly for the SA-IDDES model. Considering that it noticeably complicates the IDDES formulation (for a full description of the IDDES model see Appendix 2) and makes an analysis and understanding of the model performance non-trivial, it was tempting to evaluate the effect of removing  $f_e$  from the SST-based formulation of IDDES, i.e. setting  $f_e = 0$ . Hereafter, this model is referred to as simplified IDDES (its detailed formulation is available in Appendix 2), in contrast to IDDES, which means SST-based IDDES with  $C_{dt1} = 8$  and  $f_e$  active, considered in Section 3. The simplified IDDES has been evaluated based on a range of flows, with confined areas of attached and separated flow regions. Obtained results are presented below.

### 5.1 Developed channel flow

The simplified IDDES was first applied again to the channel flow, where the effect of omitting  $f_e$  had been expected to be most noticeable. The three flow regimes considered in Section 4.1 were simulated with the use of the problem set-up and boundary conditions described in Section 4.1. Results of the simulations in the form of the mean velocity and eddy viscosity profiles are shown in Fig. 6. The figure suggests that, in line with the expectations, the simplified IDDES does cause somewhat stronger LLM at the low and moderate values of the Reynolds number, but the effect is marginal. Thus, as far as this flow is concerned, the simplification of the original formulation of the SST-based IDDES [4] is justified.

### 5.2 Backward-facing step flow

Some results of SST-based IDDES and Simplified IDDES of this flow (see Section 3 for the description) are shown in Fig. 7. It suggests that both models perform practically identically, thus supporting the positive conclusion formulated regarding the simplified IDDES model based on the simulation of developed channel flow presented in the previous section.

### 5.3 Flow over periodic 2D hills

This flow is a popular test case for validation of turbulence models with separation and reattachment. It served as the test case of two ERCOFTAC SIG15 Workshops [14, 15] and is included in the ERCOFTAC database (case 81), where details of the geometry are given. In the present simulations, the Reynolds number based on the hill height,  $H$ , and the bulk velocity,  $U_b$ , was equal to 10600. Following Breuer et al. LES [15], the length of the computational domain was equal to  $9H$  and its size in the spanwise direction was  $4.5H$  (see Fig. 8a). The computational grid contains about 1.5 million hexahedral cells which correspond to  $161 \times 161 \times 61$  nodes in the  $x$ ,  $y$ , and  $z$  directions respectively. On the upper and lower walls of the channel no

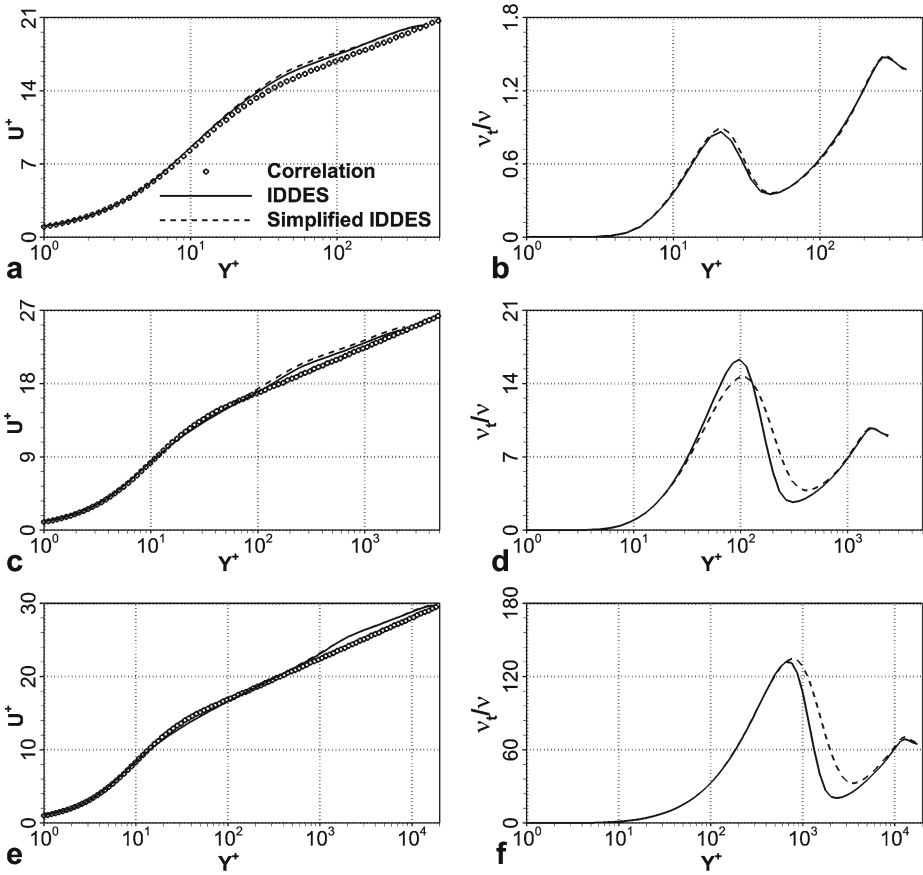


**Fig. 6** Comparison of mean velocity and eddy viscosity profiles in developed channel flow predicted by full and simplified versions of the SST-based IDDES model. **a, b**— $Re_\tau = 395$ , **c, d**— $Re_\tau = 2400$ , **e, f**— $Re_\tau = 18000$

slip-conditions were applied, whereas the boundary conditions in the spanwise and streamwise directions were set to periodic. The flow was driven by a pressure force term in the momentum equation.

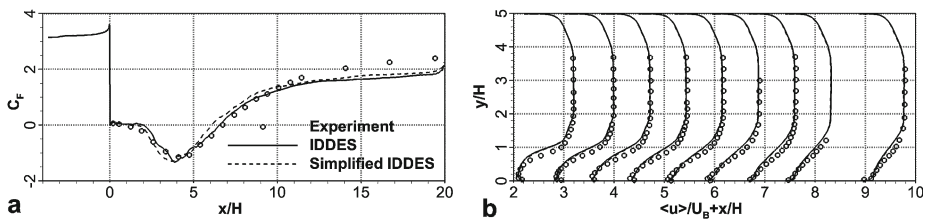


**Fig. 7** Comparison of skin friction coefficient distribution over the step-wall **a** and profiles of streamwise velocity  $\langle u \rangle$  **b** predicted by full and simplified versions of the SST- IDDES model in the BFS flow. The profiles are plotted at  $x/H = 2.2, 3.0, 3.7, 4.5, 5.2, 5.9, 6.7, 7.4, \text{ and } 8.7$

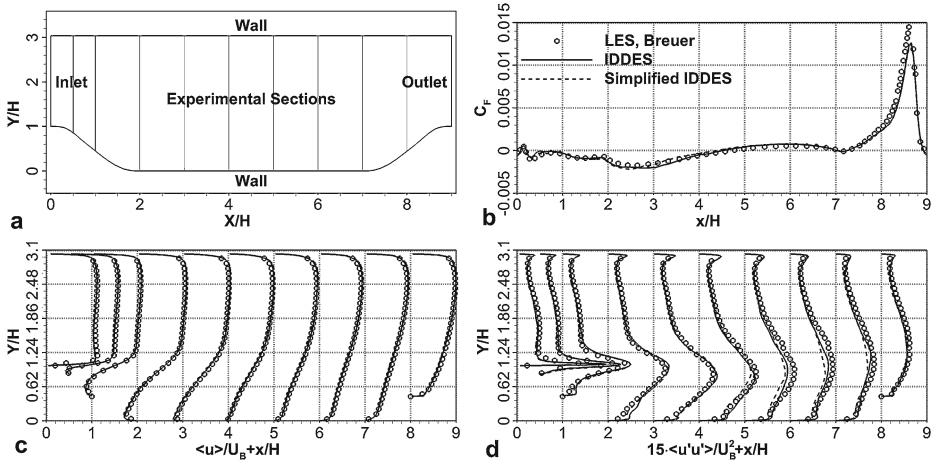


**Fig. 8** A sketch of the flow **a** and a comparison of skin friction distribution **b**, streamwise velocity profiles  $\langle u \rangle$  **c**, and normal  $\langle u'u' \rangle$  stresses **d** predicted by full and simplified versions of the SST-based IDDES model with LES data [15]. The profiles are plotted at  $x/H = 0.05, 0.5, 1, 2, 3, 4, 5, 6, 7,$  and  $8$

The grid ensured the values of  $\Delta y_w^+$  to be less than one for both the hill-wall and upper straight wall. The non-dimensional time step in the simulations was  $\Delta t = 0.02$ , which corresponds to a CFL number less than one in the entire domain.

Some results for the simulations with the use of both the original and the simplified IDDES models are presented in Fig. 8. Just as for the two flows considered above (the plane channel and BFS), both models produce virtually identical predictions of the skin friction distribution (Fig. 8b), for profiles of the mean streamwise velocity (Fig. 8c) and the normal Reynolds stresses (Fig. 8d), which all very well agree with the reference LES solution of Breuer et al. [15].

### 5.4 Wall-mounted 2D hump flow

This flow has been studied experimentally by Greenblatt et al. [16] and, similar to the flow over the periodic hills, it has been used as a benchmark in a number of CFD studies [18, 19]. The present simulations were conducted at a Reynolds number based on the free-stream velocity  $U_\infty$  and hump chord  $C$  equal to  $9.36 \cdot 10^5$ . The simulation of this flow was performed in two stages.

First, a 2D RANS computation has been carried out in the full domain (see Fig. 9a) extending from  $-2.14C$  to  $4C$  (0 corresponds to the hump beginning) with a grid of  $4.0 \cdot 10^4$  hexahedral cells. The inflow boundary conditions for RANS were imposed based on the preliminary flat plate boundary layer computations up to the flow section  $x/C = 2.14$  ( $Re_\theta = 7200$ ), where the flow parameters were measured in the experiment. Other than that, the upper (straight) wall of the channel, where the free-slip wall conditions are specified, was slightly constricted to reproduce the blockage effect of the end plates in the experimental configuration [19].

In the second, IDDES, stage of the simulation, the computational domain extended from  $0.4C$  to  $4C$  (its inlet section is placed on the hump plateau), and its

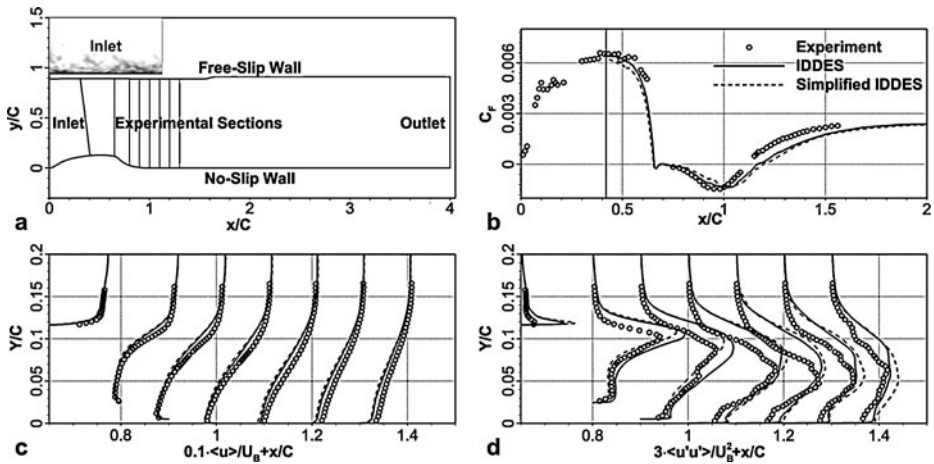


**Fig. 9** A sketch of the flow **a** and a comparison of skin friction coefficient distribution **b**, profiles of streamwise velocity  $\langle u \rangle$  **c**, and normal  $\langle u'u' \rangle$  stresses **d** predicted by full and simplified versions of SST-based IDDES model in the 2D wall-mounted hump flow with experimental data [16]. Profiles are plotted at  $x/C = 0.65, 0.8, 0.9, 1.0, 1.1, 1.2,$  and  $1.3$

size in the spanwise direction was equal to  $0.2C$ . In the spanwise direction, periodic boundary conditions were imposed.

The inflow boundary conditions were based on the RANS solution at  $x/C = 0.4$  known from the previous simulation, whereas the inflow turbulent content needed for activating the WMLES branch of the IDDES model were created with the use of a recently proposed synthetic turbulence generator [17] (see Fig. 9a for example of turbulent structures). For the turbulence quantities,  $k$  and  $\omega$ , inlet boundary conditions were specified as follows. The specific dissipation rate was taken from the RANS computation and for the turbulence kinetic energy the following equation was used:

$$k = \min(k_{RANS}, \omega_{RANS} \cdot \nu_t)$$

$$\nu_t = (C_{Smag} \cdot \min(C_w \cdot \max(d_w, h_{max}), h_{max}))^2 \cdot S$$

Here  $\nu_t$  is eddy viscosity calculated with the use of a modified Smagorinsky model [4], which uses the IDDES length scale,  $d_w$ —is the distance to the nearest wall,  $h_{max}$  is grid length scale, and  $S$ —is the strain rate invariant. The model constants are  $C_{smag} = 0.2$  and  $C_w = 0.15$ .

The computational grid in the IDDES simulation had about 1.6 million hexahedral cells with 50 cells in spanwise direction. The non-dimensional time step in the simulation was  $\Delta t = 0.001$ , which lead to a CFL number less than one in the entire domain.

Some typical results of the simulations with the use of the full and simplified versions of the SST-based IDDES model are presented in Fig. 9. They show that similar to all the flows considered above, both versions yield close solutions. However, in this case, the difference between the two solutions, especially with regard to the profiles of the normal stresses (see Fig. 9d) is somewhat more pronounced. On the other

hand, in terms of the agreement with the data, the full version, in general, does not surpass the simplified one, and therefore the simplification appears justified for this flow as well.

### 5.5 Hydrofoil with a trailing edge separation

This flow, investigated in the experiments of Blake [20], is characterized by a shallow separation bubble with separation from a smooth surface and presents a challenging test to CFD. The Reynolds number based on the free stream velocity and the hydrofoil chord is equal to  $2.2 \cdot 10^6$  or  $1.01 \cdot 10^5$  based on its thickness,  $H$ .

Similar to the two-dimensional hump considered in the previous section, the simulation of the flow was performed with the use of the two-stage, RANS-IDDES, approach. The 2D RANS computation was carried out for the entire hydrofoil (the computational domain extends from  $x/H = -60$  to  $x/H = 20$  in  $x$  direction ( $x = 0$  corresponds to the hydrofoil trailing edge) and from  $y/H = -40$  to  $y/H = 40$  in the  $y$  direction (see Fig. 10a). The RANS grid had  $1.2 \cdot 10^5$  hexahedral cells.

The IDDES domain started at  $x/H = -4$  under the hydrofoil and at  $x/H = -1$  above it and extended up to  $x/H = 20$  in the wake. Its size in the spanwise direction was equal to  $0.5H$ . In the spanwise direction, periodic boundary conditions were imposed.

The inflow boundary conditions for IDDES were based on the RANS solutions at  $x/H = -4$  under and at  $x/H = -1$  above the hydrofoil and the inflow turbulent content was again created with the use of the synthetic turbulence generator [17]. The same boundary conditions as those described in Section 5.4 were used for the turbulent properties.

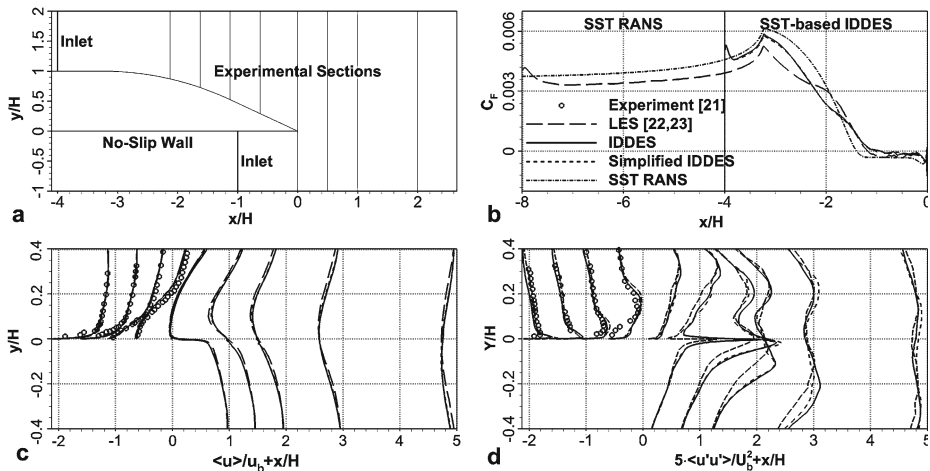


**Fig. 10** A sketch of the flow domain **a** and a comparison of skin friction coefficient distributions **b** and profiles of streamwise velocity  $\langle u \rangle$  **c** and normal stress  $\langle u'u' \rangle$  **d** predicted by full and simplified versions of SST-based IDDES model with LES results of [21, 22] and experimental data [20]. Profiles are plotted at  $x/H = -2.125, -1.625, -1.125, -0.625, 0.0, 0.5, 1.0, 2.0, \text{ and } 4.0$

The IDDES grid had about 3.5 million hexahedral cells with 50 cells in spanwise direction. The grid-steps in the streamwise and spanwise directions were equal to  $0.01H$  and  $0.01H$  respectively, and the grid in the wall-normal direction was designed so that the near-wall  $y^+$  was less than one in the entire domain. The non-dimensional time step was  $\Delta t = 0.005$  which corresponds to a CFL number less than one in the entire domain.

In Fig. 10, results of the simulations obtained using the full and simplified SST-based IDDES model versions are compared with each other. In addition, well-resolved LES (Wang and Moin [21, 22]) and experimental data [20] are included. It can be seen that, again, virtually no differences are observed between the predictions of the full and simplified versions of the SST-based IDDES models and that both agree fairly well with the LES predictions and experimental data.

### 6 Conclusions

A recalibration of the empirical constants  $C_{d1}$  and  $C_{d2}$  involved in the delay function  $f_d$  of the SA-based DDES model was carried out in order to optimize the formulation when used with the SST-based DDES model. Simulations of different flows, both attached and separated, performed with the recalibrated constants have shown that they provide the same level of shielding for the SST-based DDES and IDDES variants from model stress depletion as achieved by the SA-IDDES models on one hand, and do not impair the turbulence resolving capability of the model in the separated flow regions, on the other hand. It has also been shown that the use of these constants within the SST-based IDDES model does not corrupt its WMLES capability in the attached flow regions.

In addition, a simplified version of SST-based IDDES model is shown to perform virtually identical to its full version in all the considered flows suggesting that in the framework of the SST-based IDDES model this function is superfluous.

**Acknowledgements** The author of this paper would like to acknowledge financial support from the EU project ATAAC (Advanced Turbulence Simulation for Aerodynamic Application Challenges) funded by the European Community in the 7th Framework Programme under Contract No. ACP8-GA-2009-233710-ATAAC and from ANSYS Inc.

### Appendix 1: SST DDES Formulation

The governing equations of the SST DDES model read as [2]:

$$\begin{aligned} \frac{\partial \rho k}{\partial t} + \nabla \cdot (\rho \vec{U} k) &= \nabla \cdot [(\mu + \sigma_k \mu_t) \nabla k] + P_k - \rho \sqrt{k^3} / l_{DDES} \\ \frac{\partial \rho \omega}{\partial t} + \nabla \cdot (\rho \vec{U} \omega) &= \nabla \cdot [(\mu + \sigma_\omega \mu_t) \nabla \omega] + 2(1 - F_1) \rho \sigma_{\omega 2} \frac{\nabla k \cdot \nabla \omega}{\omega} + \alpha \frac{\rho}{\mu_t} P_k - \beta \rho \omega^2 \\ \mu_t &= \rho \frac{a_1 \cdot k}{\max(a_1 \cdot \omega, F_2 \cdot S)} \end{aligned} \tag{1}$$

In Eq. 1  $F_1$  and  $F_2$  denote the SST blending functions which read as follows:

$$\begin{aligned}
 F_1 &= \tanh(\arg_1^4) \\
 \arg_1 &= \min\left(\max\left(\frac{\sqrt{k}}{C_\mu \omega d_w}, \frac{500\nu}{d_w^2 \omega}\right), \frac{4\rho\sigma_{\omega 2} k}{CD_{k\omega} d_w^2}\right) \\
 CD_{k\omega} &= \max\left(2\rho\sigma_{\omega 2} \frac{\nabla k \cdot \nabla \omega}{\omega}, 10^{-10}\right) \\
 F_2 &= \tanh(\arg_2^2) \\
 \arg_2 &= \max\left(\frac{2\sqrt{k}}{C_\mu \omega d_w}, \frac{500\nu}{d_w^2 \omega}\right) \tag{2}
 \end{aligned}$$

Here  $d_w$  is the distance to the nearest wall. The production term in Eq. 1 reads as follows:

$$P_k = \min(\mu_t S^2, 10 \cdot C_\mu \rho k \omega) \tag{3}$$

The DDES length scale in Eq. 1 reads as follows:

$$\begin{aligned}
 l_{DDES} &= l_{RANS} - f_d \max(0, l_{RANS} - l_{LES}) \\
 l_{LES} &= C_{DES} h_{\max} \\
 l_{RANS} &= \frac{\sqrt{k}}{C_\mu \omega} \\
 C_{DES} &= C_{DES1} \cdot F_1 + C_{DES2} \cdot (1 - F_1) \tag{4}
 \end{aligned}$$

Here  $h_{\max}$  is the maximum edge length of the cell. Finally, the empiric blending function  $f_d$  in Eq. 4 is computed with the use of the following relations:

$$\begin{aligned}
 f_d &= 1 - \tanh\left[(C_{d1} r_d)^{C_{d2}}\right] \\
 r_d &= \frac{\nu_t + \nu}{\kappa^2 d_w^2 \sqrt{0.5 \cdot (S^2 + \Omega^2)}} \tag{5}
 \end{aligned}$$

Here  $S$  is the magnitude of the strain rate tensor and  $\Omega$  is the magnitude of vorticity tensor.

The model constants read as follows:

$$\begin{aligned}
 C_\mu &= 0.09, \quad \kappa = 0.41, \quad a_1 = 0.31 \\
 C_{DES1} &= 0.78, \quad C_{DES2} = 0.61, \quad C_{d1} = 20, \quad C_{d2} = 3 \tag{6}
 \end{aligned}$$

All the constants with index 3 are computed by a blend from the corresponding constants of the k- $\epsilon$  and k- $\omega$  model via  $\alpha = \alpha_1 \cdot F_1 + \alpha_2 \cdot (1 - F_1)$  etc.:

$$\begin{aligned}
 \alpha_1 &= 5/9, \quad \beta_1 = 0.075, \quad \sigma_{k1} = 0.85, \quad \sigma_{\omega 1} = 0.5 \\
 \alpha_2 &= 0.44, \quad \beta_2 = 0.0828, \quad \sigma_{k2} = 1, \quad \sigma_{\omega 2} = 0.856 \tag{7}
 \end{aligned}$$

## Appendix 2: SST IDDES Formulation

The governing equations of the SST IDDES model [2] are presented in Eqs. 1, 2, 3 with  $l_{DDES}$  replaced by  $l_{IDDES}$  in Eq. 1. The IDDES length scale in Eq. 1 reads as follows:

$$\begin{aligned}
 l_{IDDES} &= \tilde{f}_d \cdot (1 + f_e) \cdot l_{RANS} + (1 - \tilde{f}_d) \cdot l_{LES} \\
 l_{LES} &= C_{DES} \Delta \\
 l_{RANS} &= \frac{\sqrt{k}}{C_\mu \omega} \\
 C_{DES} &= C_{DES1} \cdot F_1 + C_{DES2} \cdot (1 - F_1)
 \end{aligned} \tag{8}$$

The LES length-scale  $\Delta$  is defined as:

$$\Delta = \min \{ C_w \max [d_w, h_{\max}], h_{\max} \} \tag{9}$$

Here  $h_{\max}$  is the maximum edge length of the cell. Finally, the empiric blending function  $\tilde{f}_d$  in Eq. 8 is computed with the use of the following relations:

$$\begin{aligned}
 \tilde{f}_d &= \max \{ (1 - f_{dt}), f_b \} \\
 f_{dt} &= 1 - \tanh \left[ (C_{dt1} \cdot r_{dt})^{C_{dt2}} \right] \\
 r_{dt} &= \frac{\nu_t}{\kappa^2 d_w^2 \sqrt{0.5 (S^2 + \Omega^2)}} \\
 f_b &= \min \{ 2 \exp(-9\alpha^2), 1.0 \} \\
 \alpha &= 0.25 - d_w / h_{\max}
 \end{aligned} \tag{10}$$

In original model formulation the elevating function  $f_e$  in Eq. 8 reads as follows:

$$\begin{aligned}
 f_e &= f_{e2} \cdot \max ((f_{e1} - 1.0), 0.0) \\
 f_{e1} &= \begin{cases} 2 \cdot \exp(-11.09 \cdot \alpha^2), & \alpha \geq 0 \\ 2 \cdot \exp(-9.0 \cdot \alpha^2), & \alpha < 0 \end{cases} \\
 f_{e2} &= 1.0 - \max (f_t, f_l) \\
 f_t &= \tanh \left( (C_t^2 \cdot r_{dt})^3 \right) \\
 f_l &= \tanh \left( (C_l^2 \cdot r_{dl})^{10} \right) \\
 r_{dl} &= \frac{\nu}{\kappa^2 d_w^2 \sqrt{0.5 (S^2 + \Omega^2)}}
 \end{aligned} \tag{11}$$

In simplified version of IDDES  $f_e$  function in Eq. 8 is set to zero, thus the IDDES length scale reads as follows:

$$l_{IDDES} = \tilde{f}_d \cdot l_{RANS} + (1 - \tilde{f}_d) \cdot l_{LES} \tag{12}$$

In addition to the model constants in Eqs. 6 and 7 the following constants are introduced in the model:

$$C_w = 0.15, C_{dt1} = 20, C_{dt2} = 3, C_l = 5.0, C_t = 1.87 \quad (13)$$

## References

1. Fröhlich, J., Von Terzi, D.: Hybrid RANS/LES methods for the simulation of turbulent flows. *Prog. Aerosp. Sci.* **44**, 349–377 (2008)
2. Menter, F.R., Kuntz, M., Langtry, R.: Ten years of experience with the SST turbulence model. 4th International Symposium on Turbulence Heat and Mass Transfer, pp. 625–632 (2003)
3. Spalart, P.R., Deck, S., Shur, M.L., Squires, K.D., Strelets, M.K., Travin, A.: A new version of detached-eddy simulation, resistant to ambiguous grid densities. *Theor. Comput. Fluid Dyn.* **20**, 181–195 (2006)
4. Shur, M.L., Spalart, P.R., Strelets, M.K., Travin, A.K.: A hybrid RANS-LES approach with delayed-DES and wall-modeled LES capabilities. *Int. J. Heat Fluid Flow* **29**, 1638–1649 (2008)
5. ANSYS FLUENT 12.0 Theory Guide, ANSYS Inc. (2009)
6. Rhie, C.M., Chow, W.L.: Numerical study of the turbulent flow past an airfoil with trailing edge separation. *AIAA J.* **21**, 1525–1532 (1983)
7. Dukowicz, J.K., Dvinsky, A.S.: Approximate factorization as a high-order splitting for the implicit incompressible flow equations. *J. Comput. Phys.* **102**, 336–347 (1992)
8. Armsfield, S., Street, R.: The fractional-step method for the Navier-Stokes equations on staggered grids: accuracy of three variations. *J. Comput. Phys.* **153**, 660–665 (1999)
9. Spalart, P.R., Jou, W.H., Strelets, M., Allmaras, S.R.: Comments on the feasibility of LES for wings, and on a hybrid RANS/LES approach. In: Proceedings of first AFOSR international conference on DND/LES (1997)
10. Vogel, J.C., Eaton, J.K.: Combined heat transfer and fluid dynamic measurements downstream of a backward-facing step. *J. Heat Mass Transfer* **107**, 922–929 (1985)
11. Strelets, M.: Detached Eddy simulation of massively separated flows. *AIAA J.* **2001-0879**, 1–18 (2001)
12. Reichardt, H.: Vollständige darstellung der turbulenten geschwindigkeitsverteilung in glatten leitungen. *Z. Angew. Math Mech.* **31**, 208–219 (1951)
13. Simpson, R.L., Long, C.H., Byun, G.: Study of vortical separation from an axisymmetric hill. *Int. J. Heat Fluid Flow* **23**, 582–591 (2002)
14. Temmerman, L., Leschziner, M.A.: Large eddy simulation of separated ow in a streamwise periodic channel constriction. In: *Int. Symp. Turb. Shear Flow Phenomena*, Stockholm, Sweden (2001)
15. Breuer, M., Peller, N., Rapp, C., Manhart, M.: Flow over periodic hills—numerical and experimental study in a wide range of Reynolds numbers. *Comput. Fluid* **38**, 433–457 (2009)
16. Greenblatt, D., Paschal, K.B., Chung-Sheng, Y., Harris, J.: A separation control CFD validation test case Part 2. Zero efflux oscillatory blowing. *AIAA Pap.* **2005-0485**, 1–24 (2005)
17. Adamian, D., Travin, A.: An Efficient Generator of Synthetic Turbulence at RANS-LES Interface in Embedded LES of Wall-Bounded and Free Shear Flows. *ICCFD6* (2010)
18. Avidis, A., Lardeau, S., Leschziner, M.: Large Eddy simulation of separated flow over a two-dimensional hump with and without control by means of a synthetic slot-jetle. *Flow Turbul. Combust.* **83**, 343–370 (2009)
19. Rumsey, C.L., Gatski, T.B., Sellers, W.L., Vatsa, V.N., Viken, S.A.: Summary of the 2004 CFD Validation Workshop on Synthetic Jets and Turbulent Separation Control. *AIAA Pap.* **2004-2217**, 1–31 (2004)
20. Blake, W.K.: A statistical description of pressure and velocity fields the trailing edge of a flat strut. David Taylor Naval Ship R & D Center Report 4241, Bethesda (1975)
21. Wang, M., Moin, P.: Dynamic wall modeling for large-eddy simulation of complex turbulent flows. *Phys. Fluid* **14**, 2043–2051 (2002)
22. Wang, M., Moin, P.: Computation of trailing-edge flow and noise using Large-Eddy Simulation. *AIAA J.* **38**, 2201–2209 (2000)